Miniature snapshot mid-infrared spectrometer based on metal-insulator-metal metasurface

IOP Publishing Journal of Optics
J. Opt. **26** (2024) 085003 (8pp) https://doi.org/10.1088/2040-8986/ad5359

Miniature snapshot mid-infrared spectrometer based on metal-insulator-metal metasurface

Weijun Liu[1], Yuanqing Wan[1], Haoxiang Yu[1], Quan Yuan[1], Tianyue Li[1], Fang Xue[2] and Shuming Wang[1,3,*]

[1] National Laboratory of Solid State Microstructures, School of Physics, Nanjing University, Nanjing 210093, People's Republic of China
[2] China Academy of Space Technology, Beijing 100080, People's Republic of China
[3] Key Laboratory of Intelligent Optical Sensing and Manipulation Ministry of Education, Nanjing University, Nanjing 210093, People's Republic of China

E-mail: wangshuming@nju.edu.cn

Received 1 February 2024, revised 13 April 2024
Accepted for publication 3 June 2024
Published 3 July 2024

Abstract

Metasurfaces showcase the performance of light field manipulation at the subwavelength scale, generating tremendous applications in the field of optical imaging and sensing, especially in spectroscopic detection. Here, we demonstrate a spectral detector comprising metal-insulator-metal composite structures working in the mid-infrared band, which can effectively collect and restore target spectral characteristics in the mid-infrared band with a trained reconstruction algorithm. The proposed device consists of snapshot multichannel detection and spectral reconstruction, showing an average spectral reconstruction accuracy approaching 80% of the system. Moreover, we discuss the feasibility of applying this structural design to a miniature spectrometer over a wider infrared wavelength range by proposing a feasible design strategy. Our results provide a novel approach for low-cost and portable mid-infrared spectroscopic detection in ultracompact mid-infrared spectral imaging and sensing elements.

Supplementary material for this article is available online

Keywords: multi-layered microstructure, metasurface, spectral reconstruction, dynamic spectral detection

1. Introduction

Light carries abundant information containing amplitude, polarization, phase, time and wavelength among which spectral information tightly refers to the field distribution in the wavelength dimension. For example, the structural composition of an object determines the spectral information of emitted or reflected light within the given light source and surroundings. Therefore, the spectral feature is the inherent characteristics of the objects, which can be exploited for the analysis of the spectrum chemical composition and internal microstructure of the substance with the broaden applications on material analysis, food safety, medical diagnosis, and biological imaging [1–4]. Generally, spectrometers usually consist of prisms, gratings, and other devices to split the dispersion between different optical paths. However, due to the diffraction effect, the inverse relationship between spectral resolution and the optical path leads to the large size, low integration, and high costs of the spectrometer system; hence, the compact spectrometers with integrated partials are in great need. Driven by this demand, the Fourier-transform spectrometers

* Author to whom any correspondence should be addressed.

[5, 6] have been proposed in recent years to reduce the volume of spectroscopic devices; some spectral detection equipment utilizing microring resonators [6–8] and optical waveguide coupling [9] have also demonstrated excellent performance. These spectral detection devices can maintain high spectral resolution and high signal-noise ratio (SNR), but their spectral resolution is severely limited by the manufacturing process. Meanwhile, due to the creeping speed of data processing, constraining the detection for a wide range of dynamic spectral information is required.

In recent years, thanks to the development of computational imaging [10, 11] and broad applications of machine learning in the imaging field [11, 12], the spectral detectors based on broadband filter arrays and spectral computational reconstruction methods have been remarkably developed whose spatial pixel is divided into several detection channels, each with different broadband spectral response characteristics. Then, the target channels are realized by space periodical or time-adjustable microstructure arrays such as photonic crystal plates [13], voltage-regulated van der Waals junctions [14], colloidal quantum dots [15], and metasurface elements [16, 17]. In addition, there are some spectrometers that use the idea of coding, which encode the spatial and spectral information of the incident light at the same time by building a spatial mask to realize the reconstruction and detection of three-dimensional (3D) or even four-dimensional (4D) information using reconstruction algorithms after detecting the encoded image information [18–20]. Among them, metasurfaces as large-area nanostructures comprising small subwavelength units, with its characteristics of strong plasticity, flexibility, and convenience in integration, have achieved efficient light field generation [21–25] and manipulation [26–31] with a broad application in the field of spectral detection [32–34]. Therefore, metasurfaces are suitable for flexible design according to the requirements in different working bands, whereas specific metal or dielectric structures can also respond at specific wavelengths, which can be designed and manipulated to produce varied kinds of spectral filter modulation characteristics with diverse morphology, thus further enhancing the spectral reconstruction ability of detectors.

In this work, we propose a miniaturized snapshot spectrometer operating in the mid-infrared band based on a broadband filtering scheme. The filter element of the proposed spectrometer consists of metal-dielectric-metal (MIM) composite structure array, which can work in the mid-wave infrared band of 3–5 μm to achieve a wide spectrum of filtering characteristic curves with different morphologies. The filters can shrink into a photosensor chip without additional imaging partials by designing and simulating the process of collecting field intensity data theoretically and processing spectra with reconstructing algorithms, as well as built experimental equipment to verify the spectral detection performance of our proposed detector architecture. Our results demonstrate that the proposed spectral detector only needs to take one picture to complete the spectral detection and reconstruction of a given image, and finally achieves the reconstruction of broad-spectrum spectral information in the mid-infrared band with an average accuracy of more than 80%. We believe that the proposed spectral detector has the characteristics of high integration and fast spectral detection speed, which effectively fill the blanks of a micro-detector and dynamic detection in the mid-wave infrared regime.

2. Methods and design

2.1. Principle of broadband filter and reconstruction

Figure 1(a) illustrates the scheme of our spectral detection system. The conceived metasurface spectral detection system includes a mid-infrared photoelectric image sensor and a layer of metasurface array. Each spatial pixel of the metasurface is divided into four detection channels and periodically arranged, as shown in figure 1(b). The incident light passes through the metasurface and focuses on the image sensor chip to convert into electrical signals. If the spectral response of each detection channel is $X_i(\lambda), i = 1, 2, 3, \ldots, N$, the absorption response of a mid-infrared photoelectric image sensor denotes as $A(\lambda)$, then the intensity Y_i collected by the original spectral characteristic of $F(\lambda)$ can be described as [16, 17, 34]:

$$Y_i = \int_{\lambda_1}^{\lambda_2} F(\lambda) X_i(\lambda) A(\lambda) \mathrm{d}\lambda + e_i \tag{1}$$

where e_i represents the noise signal. Let $f(\lambda)$, $x_i(\lambda)$, and $a(\lambda)$ be depicted as discrete samples $F(\lambda), X_i(\lambda)$, and $A(\lambda)$, respectively, then the discrete form of Y_i can be written as follows:

$$Y_i = \sum_{\lambda} f(\lambda) x_i(\lambda) a(\lambda) + e_i. \tag{2}$$

The spectral response characteristics of each target channel are defined by design, and the absorption response of the photoelectric sensor can be determined in advance. Let $r_i(\lambda) = x_i(\lambda) a(\lambda)$, then we get the following relation:

$$Y(i) = \sum_{\lambda} f(\lambda) r_i(\lambda) + e_i \tag{3}$$

where $Y \in R^{N\times 1}$, $R \in R^{N\times M}$, and $F(\lambda) \in R^{M\times 1}$. Equation (3) can be written in the matrix form $Y = \mathrm{RF}(\lambda) + \mathrm{e}$. Thus, the reconstruction to acquire the original spectrum of incident light is used to solve these equations.

In the process of spectral detection of each pixel, M sampling points are reconstructed using a one-dimensional (1D) vector consisting of field intensity values recorded by N measurement channels, whereas $N < M$ makes this as an underdetermined problem that is theoretically impossible to obtain a strictly accurate solution based on these data [35, 36]. However, the original spectrum of an object and the undersampling process from the original spectrum to the measurement data have many hidden regulations, and if broadband filter channels can agree with the sparsity requirements of

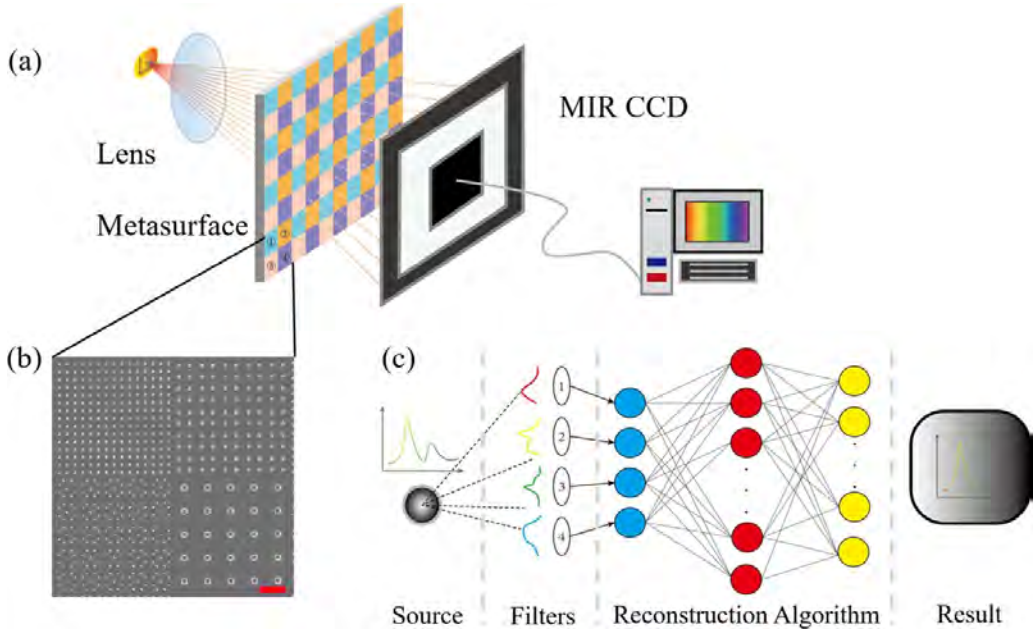

Figure 1. Schematic diagram of the architecture of the proposed spectral imaging system. (a) Individual components of the imaging system. (b) SEM scans of the metasurface broadband filter. Scale bar: 3 μm. (c) Process of spectral reconstruction.

compressed sensing theory, it is possible to break through the limitations of Nyquist's sampling theorem [37]. Although some methods have proven that can be adopted in the spectral calculation and reconstruction process, one can obtain an approximation with acceptable error [35, 36]. Recently, the inversion calculation using deep learning has become an important computational reconstruction method, and artificial neural network algorithms can efficiently identify and learn implicit associations between the input and output datasets, which is very suitable for spectral reconstruction. Here, we use a neural network algorithm to discretely sample the spectral information on each spatial pixel, and the obtained light intensity information can be used as the input vector. A set of discrete spectral data can be obtained through the reconstruction algorithm. In the end, the reconstructed spectral curve can be achieved by interpolation fitting, as shown in figure 1(c). Using such a detection system, the information on each spatial pixel is processed in the same way, and detection and reconstruction of spectral information of the object can be realized after combination. Compared with traditional computing methods, the deep neural network applied here has two advantages: first, the speed of spectral reconstruction can be several orders of magnitude faster, which is conducive to agree with the need for dynamic image acquisition. The other is that prior knowledge about coding is no longer needed, only requiring enough rich and comprehensive samples in the training process; therefore, well-trained deep neural networks have excellent reconstruction accuracy and denoising ability. However, deep learning requires suitable datasets as training data, and parameter selection exerts a great impact on reconstruction results. Therefore, it is a key step for us to select an appropriate and sufficient dataset to train the neural network according to a specific application environment [38].

2.2. *Metasurface detector design*

According to the above analysis, there are two important steps to achieve spectral imaging using metasurface broadband filtering: the first step is to design a detection channel with randomly distributed broadband spectral response curves, and the second step is to train an algorithm to reconstruct the spectrum based on the design. Due to the particularity of the underdetermined equation solution and the requirements of sparse sampling, the more evident the spectral response curve characteristics, the higher the spectral reconstruction ability. Therefore, the focus of the design is to determine a series of metasurface microstructure array designs with obvious spectral response characteristics and large enough differences between them.

Surface plasmon (SP) can limit the electromagnetic field energy to the subwavelength scale [39], overcoming the classical diffraction limit and providing an essential solution for miniaturized light field manipulation. Meanwhile, multiple resonances in the local region can interact with each other; therefore, the coupling mode of the whole system can be used to obtain significant responses of transmittance with the wavelength of the light, so the specific effect is strongly correlated with the incident light frequency and arrangement pattern of SP [39, 40]. Because of the above characteristics, we use the MIM strategy to build unit cells, which are sandwich-shaped columns placed on a substrate, containing

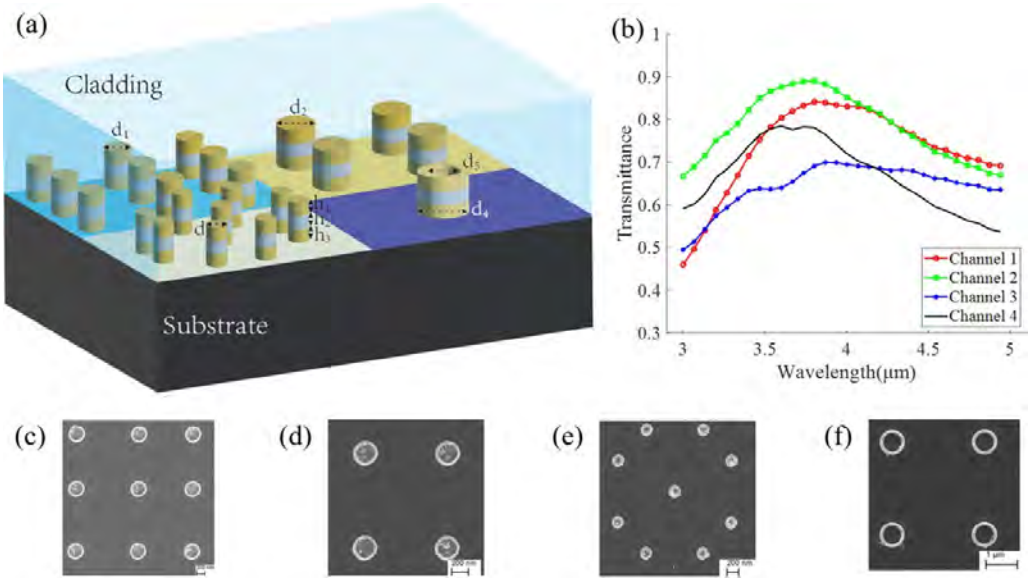

Figure 2. Design of metasurface and transmittance-wavelength response of each detection channel. (a) Microstructures in four detection channels. Structural parameters: $d_1 = 300$ nm, $d_2 = 400$ nm, $d_3 = 200$ nm, $d_4 = 800$ nm, $d_5 = 600$ nm, $h_1 = 70$ nm, $h_2 = 60$ nm, $h_3 = 70$ nm. In each individual column, the uppermost and lowest material is gold, and the middle material is germanium, as displayed in different colors in the diagram. (b) The transmittance-wavelength response relationship of the four channels given by simulation. (c)–(f) SEM images of each detection channel.

two layers of a metal and an insulator sandwiched between them. The shape parameters such as length, width, cross-sectional radius, and thickness can be specifically adjusted. Numerical calculations show that when such a microstructure is illuminated by a plane wave, multiple resonant modes are excited and coupled between the upper and lower layers of metals [40, 41]. By changing the structure and arrangement of the MIM, the transmittance curve can be adjusted using a large extent. Considering the coupling response between adjacent structural columns, such microstructures can be easily designed to form rich transmittance curves over a small metasurface area, such as peaks and troughs in the spectral response curves and different curve trends, which are very conducive to the spectral reconstruction [36]. In this scenario, the metasurface is insensitive to the polarization. Therefore, we only use C_4 symmetry-protected structures with the cross-section of circles or concentric rings. This increases the overall transmittance of the device and avoids incompatibility between our detection system and other optical components.

In the mid-infrared band, traditional materials (such as silica, among others) that are commonly used to build metasurface arrays will become opaque. The spatial size of the structure must reach the subwavelength scale close to 3–5 μm to use the MIM microstructure to produce a strong enough response characteristic. Considering the material characteristics and the ease of processing and manufacturing, we choose germanium as a substrate and dielectric material, and gold as a metal layer material due to its stability in air. The designed four-channel metasurface cellular structure is shown in figure 2(a). During the design, we first design basic styles for a variety of unit cells in Finite-Difference Time-Domain simulation by a rough calculation, and then optimize the structural parameters such as the radius, height, and layout position of the microstructure to obtain a design scheme with the best local average transmittance and the strongest fluctuation of transmittance with wavelength.

We first identify a number of possible arrangements for microstructure columns, such as $n \times n$ cylindrical equidistant arrays, cross-shaped arrangements, and the replacement of some of these columns with rings. Note that this is only a simple classification of the relative positions between the microstructures, and the specific structural parameters, such as the height, radius, and spacing of the microstructure columns, in between can be adjusted within the range allowed by the processing and manufacturing process. We iterate over these parameters at regular intervals and simulate and compare the transmittance-spectral response curves of the metasurface structures under each configuration.

Then, we compared and screened the optimization results of various design schemes to determine the periodic structure design of the four detection channels that best meet the needs of spectral reconstruction. Finally, we obtained a series of detection channel designs with an average transmittance of $\geqslant$60% and standard deviation ($s = \sqrt{\sum (x_i - \bar{x})^2}$, $i = 1, 2, 3, \ldots$,) of the transmittance-wavelength response relationship between the four channels are all greater than 0.05.

All eligible metasurface design combinations were measured by Pearson's correlation coefficient between the channels to select the one with a higher degree of uncorrelation; finally, the optimal design was obtained (supplementary material S2). The transmittance-wavelength response curves of the designed four-channel microstructure cells in the working band are shown in figure 2(b). Figures 2(c)–(f) shows the SEM images of the four-channel structures. In each pixel, the arrangement

of the microstructure in each cell can be seen in supplementary material S1.

3. Results

3.1. Blackbody radiation spectroscopy detection

In our tentative scheme, the proposed spectral detector is primarily used to detect spectral information of thermal light source, and the target object is approximately a blackbody with a temperature between 300 K to 1000 K. To verify the feasibility of spectral reconstruction of the proposed system, the theoretical verification of spectral reconstruction was performed first. First, we used a commercial Fourier-Transform Infrared spectrometer to calibrate the transmittance-wavelength response relationship of the designed metasurface filter unit, and the results show that the detection channels were in good agreement with the design simulation results, as shown in figure 3(a).

According to simulation results of the four detection channels' transmittance-wavelength response relationship, we simulated and calculated the spectral detection reconstruction process in one pixel. First, we created a database of several mid-infrared spectral curves; from which each time, we randomly divided the training samples that were the output vectors of the neural network.

During training, all the raw spectral data are derived from the radiation characteristic curves of the blackbody randomly selected from the temperature values in the range of 200 K $\sim$ 1500 K, as well as from the linear combination of its translational transformation and multiple radiation curve characteristic curves. All spectral data were normalized to a total of 6000 sets of data. The training data were all blackbody radiation spectra because our main focus is on the spectral detection task where the target is the blackbody radiation, and the training data with the same characteristics as the target can save the training time and maximize the accuracy of spectral reconstruction.

The construction and training of the neural network used, and the processing of the data, are all performed in MATLAB. More information on the algorithm can be found in supplementary material S4. The spectral data were convoluted with the transmittance-wavelength response relationship of the four channels, and the light intensity that can be detected by the four channels is calculated, which is used as input vector of the neural network. Subsequently, the training set, verification set, and test set were randomly demarcated many times until the neural network algorithm was fully trained and reconstruction accuracy tended to be stable. Finally, the smoothed curve is plotted by using the Lagrange interpolation method as the detection result of the spectrum. We randomly selected several sets of reconstructed spectral data to be compared with the original spectral data, as shown in figures 3(b) and (c).

We quantified the effect of the analysis by comparing the differences between the data and the shape of the curve and calculating the spectral vector difference from each set of spectral data pairs. The spectral curve reconstruction results for the entire dataset were synthesized, and the average accuracy was 96%. Using this spectral reconstruction algorithm, the theoretical frames per second of the mid-infrared image containing 320 $\times$ 240 pixels can reach about 26. In summary, the simulation results demonstrate the feasibility of the proposed system for spectral detection.

In addition, in actual spectral measurement work, the system will inevitably be affected by ambient noise, and errors may also be introduced by other components in the detection optical path. According to the relevant theories in machine learning science [11, 12], the selection and adjustment of appropriate training data for the target spectrum can greatly reduce the systematic error and improve the accuracy of spectrum reconstruction. A certain proportion of random noise is introduced into the measurement to simulate the systematic error in the actual application environment, and the spectral reconstruction results under the influence of noise are given in figure 3(c), and the reconstruction accuracy is calculated. The results show that the reconstruction algorithm can resist the influence of random noise within a certain range, and the average accuracy reaches more than 80% when SNR is above 10 dB so as to achieve more accurate spectral reconstruction.

3.2. Broadband infrared spectrometer design

Based on this idea, we further envisage a spectral detector suitable for a wider band. At present, the detection needs in the infrared band are mainly concentrated in near-infrared (1–3 μm), mid-infrared (3–5 μm), and far-infrared (8–10 μm). We hope to propose an integrated detection system that can respond to the spectral characteristics from near-infrared to far-infrared at the same time, so as to reconstruct the calculation. Due to the working principle of MIM microstructure used here, it can only produce strong resonant coupling to light with similar wavelength and structural parameters, but the effect of light control with large wavelength difference is not obvious. However, the spatial resolution of the imaging system limits the size of each detection channel and even the structure of the microstructure, making it impossible to simply scale up to the same size as the wavelength of far-infrared light.

In our design, each detection channel is 15 μm^2 larger with microstructure cells periodically arranged inside. It is challenging to create a variety of spectral signature responses in all wavelength bands using a single-layer metasurface. Therefore, we combine the two layers of a metasurface to achieve the desired transmittance-spectral response relationship, as shown in figures 4(a)–(d). The upper and lower layers of the metasurface are designed based on the spectral features of the near- and far-infrared, respectively; they can respond to spectral features over a wide range of wavelengths when combined. Performance parameters such as average transmittance and variability of the design results are optimized to ensure that the multilayer structure does not affect spectral detection capabilities. The transmittance-wavelength response relationship of the four channels is shown in figure 4(e).

Using the same method, we simulated the spectral reconstruction of this design scheme, using the luminous intensity

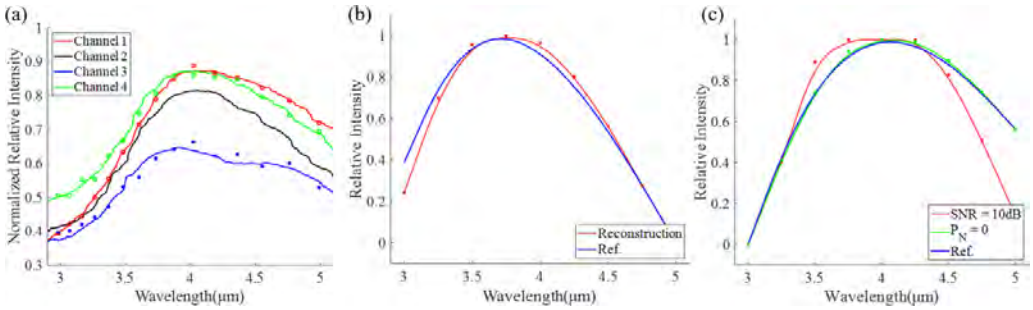

Figure 3. (a) Experimental measurement of four-channel transmittance-wavelength response relationship. (b) Results of spectral reconstruction on simulated dataset. (c) Reconstruction result with signal-to-noise ratio (SNR) = 10 dB or without noise ($P_N = 0$).

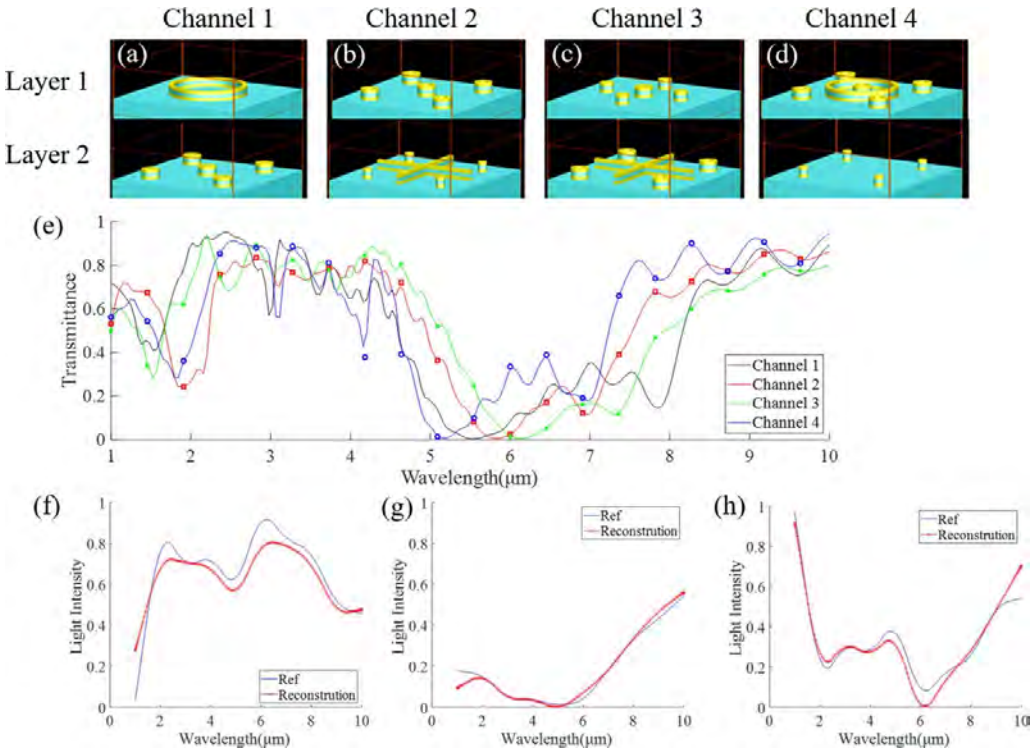

Figure 4. Broadband metasurface filter design. (a)–(d) Each detection channel is composed of two layers of metasurface microstructure. (e) The transmittance-wavelength response relationship of the four channels given by simulation. (f)–(h) Random spectrum reconstruction result.

detected by the four channels to reconstruct the random incident spectrum, and the results showed that the average accuracy of the spectral reconstruction is still above 80%, as shown in figures 4(f)–(h).

4. Discussion

In summary, based on the detection scheme of sparse sampling combined with computational reconstruction, we propose an integrated miniature spectrometer to detect spectral information of incident light in mid-infrared 3–5 μm band. In our system, the MIM microstructure array is used to construct detection channels of different transmittance-spectral response relationships. Thus, the light intensity collected by the four channels is a sparse sampling of the incident light spectrum. Considering the reconstruction accuracy, spatialresolution and detection speed, the proposed system architecture offers unique advantages in dynamic detection scenario.

Meanwhile, the specially designed and trained neural network algorithm can identify data features, calculate a set of spectral intensity values at specific locations with sufficient accuracy, and fit to obtain spectral reconstruction results to realize snapshot spectral detection of spatial images. The system is based on metasurfaces integrated on the surface of an image sensor, which is small in size and has a high light utilization rate, making it possible to combine them with integrated optical system components such as photonic chips or optical fibers to achieve additional detection capabilities. The spectral detection scheme can be extended to a wider wavelength range to achieve rapid detection of spectral features or signals,

which has important application value in the fields of infrared communication, Raman spectral detection, dynamic spectral acquisition, motion detection and so on.

Data availability statement

All data that support the findings of this study are included within the article (and any supplementary files).

Acknowledgments

This work was supported by the National Program on Key Basic Research Project of China (2022YFA1404300), National Natural Science Foundation of China (Nos. 12325411, 62288101 and 11774162), The Open Research Fund of the State Key Laboratory of Transient Optics and Photonics, Chinese Academy of Sciences (SKLST202218), the Fundamental Research Funds for the Central Universities (020414380175). Postgraduate Research & Practice Innovation Program of Jiangsu Province (KYCX23_0096).

Author contribution

W L, Y W, and H Y contributed equally to this research. S W conceived the original idea. W L developed the design and optimization of the metasurface. Y W and W L performed the fabrication of the metasurface. W L, Y W, and H Y developed the measurement and data analysis of the experiment. Q Y , T L and S W modify the manuscript. S W and X F supervised the research. All the authors discussed on the contents and prepared the manuscript.

Conflict of interest

The authors declare no competing financial interests.

ORCID iD

Shuming Wang https://orcid.org/0000-0002-0191-407X

References

[1] Gowen A, Odonnell C, Cullen P, Downey G and Frias J 2007 Hyperspectral imaging—an emerging process analytical tool for food quality and safety control *Trends Food Sci. Technol.* **18** 590–8
[2] Jia J, Wang Y, Chen J, Guo R, Shu R and Wang J 2020 Status and application of advanced airborne hyperspectral imaging technology: a review *Infrared Phys. Technol.* **104** 103115
[3] Erkinbaev C, Derksen K and Paliwal J 2019 Single kernel wheat hardness estimation using near infrared hyperspectral imaging *Infrared Phys. Technol.* **98** 250–5
[4] Mishra G, Panda B K, Ramirez W A, Jung H, Singh C B, Lee S-H and Lee I 2022 Application of SWIR hyperspectral imaging coupled with chemometrics for rapid and non-destructive prediction of Aflatoxin B1 in single kernel almonds *LWT* **155** 112954
[5] le Coarer E, Blaize S, Benech P, Stefanon I, Morand A, Lérondel G, Leblond G, Kern P, Fedeli J M and Royer P 2007 Wavelength-scale stationary-wave integrated Fourier-transform spectrometry *Nat. Photon.* **1** 473–8
[6] Zheng S N, Zou J, Cai H, Song J F, Chin L K, Liu P Y, Lin Z P, Kwong D L and Liu A Q 2019 Microring resonator-assisted Fourier transform spectrometer with enhanced resolution and large bandwidth in single chip solution *Nat. Commun.* **10** 2349
[7] Nitkowski A, Chen L and Lipson M 2008 Cavity-enhanced on-chip absorption spectroscopy using microring resonators *Opt. Express* **16** 11930–6
[8] Zhang L, Zhang M, Chen T, Liu D, Hong S and Dai D 2022 Ultrahigh-resolution on-chip spectrometer with silicon photonic resonators *Opt.—Electron. Adv.* **5** 210100–1
[9] Hartmann W, Varytis P, Gehring H, Walter N, Beutel F, Busch K and Pernice W 2020 Waveguide-integrated broadband spectrometer based on tailored disorder *Adv. Opt. Mater.* **8** 1901602
[10] Ghamisi P *et al* 2017 Advances in hyperspectral image and signal processing *IEEE Geosci. Remote Sens. Mag.* **5** 37–78
[11] Zhang J G, Su R, Fu Q, Ren W, Heide F and Nie Y 2022 A survey on computational spectral reconstruction methods from RGB to hyperspectral imaging *Sci. Rep.* **12** 11905
[12] Huang L Q, Luo R, Liu X and Hao X 2022 Spectral imaging with deep learning *Light Sci. Appl.* **11** 61
[13] Wang Z *et al* 2019 Single-shot on-chip spectral sensors based on photonic crystal slabs *Nat. Commun.* **10** 1020
[14] Yoon H H *et al* 2022 Miniaturized spectrometers with a tunable van der Waals junction *Science* **378** 396–9
[15] Bao J and Bawendi M G 2015 A colloidal quantum dot spectrometer *Nature* **523** 67–70
[16] Xiong J *et al* 2022 Dynamic brain spectrum acquired by a real-time ultraspectral imaging chip with reconfigurable metasurfaces *Optica* **9** 461–8
[17] Yang J W *et al* 2022 Ultraspectral imaging based on metasurfaces with freeform shaped meta-atoms *Laser Photon. Rev.* **16** 2100663
[18] Gehm M E, John R, Brady D J, Willett R M and Schulz T J 2007 Single-shot compressive spectral imaging with a dual-disperser architecture *Opt. Express* **15** 14013–27
[19] Yako M, Yamaoka Y, Kiyohara T, Hosokawa C, Noda A, Tack K, Spooren N, Hirasawa T and Ishikawa A 2023 Video-rate hyperspectral camera based on a CMOS-compatible random array of Fabry-Perot filters *Nat. Photon.* **17** 218–23
[20] Hua X *et al* 2022 Ultra-compact snapshot spectral light-field imaging *Nat. Commun.* **13** 2732
[21] Yu N F, Genevet P, Kats M A, Aieta F, Tetienne J-P, Capasso F and Gaburro Z 2011 Light propagation with phase discontinuities: generalized laws of reflection and refraction *Science* **334** 333–7
[22] Sun S L, He Q, Xiao S, Xu Q, Li X and Zhou L 2012 Gradient-index meta-surfaces as a bridge linking propagating waves and surface waves *Nat. Mater.* **11** 426–31
[23] Li T Y, Li X, Yan S, Xu X, Wang S, Yao B, Wang Z and Zhu S 2021 Generation and conversion dynamics of dual bessel beams with a photonic spin-dependent dielectric metasurface *Phys. Rev. Appl.* **15** 014059
[24] Fan Q B *et al* 2019 Broadband generation of photonic spin-controlled arbitrary accelerating light beams in the visible *Nano Lett.* **19** 1158–65
[25] Devlin R C, Ambrosio A, Rubin N A, Mueller J P B and Capasso F 2017 Arbitrary spin-to-orbital angular momentum conversion of light *Science* **358** 896–900
[26] Wang S M *et al* 2018 A broadband achromatic metalens in the visible *Nat. Nanotechnol.* **13** 227–32

[27] Wang S M *et al* 2017 Broadband achromatic optical metasurface devices *Nat. Commun.* **8** 187
[28] Li T Y, Xu X, Fu B, Wang S, Li B, Wang Z and Zhu S 2021 Integrating the optical tweezers and spanner onto an individual single-layer metasurface *Photon. Res.* **9** 1062–8
[29] Li T Y, Kingsley-Smith J J, Hu Y, Xu X, Yan S, Wang S, Yao B, Wang Z and Zhu S 2023 Reversible lateral optical force on phase-gradient metasurfaces for full control of metavehicles *Opt. Lett.* **48** 255–8
[30] Mueller J P B, Rubin N A, Devlin R C, Groever B and Capasso F 2017 Metasurface polarization optics: independent phase control of arbitrary orthogonal states of polarization *Phys. Rev. Lett.* **118** 113901
[31] Li T, Chen Y, Fu B, Liu M, Wang J, Gao H, Wang S and Zhu S 2024 Spin-selective trifunctional metasurfaces for deforming versatile nondiffractive beams along the optical trajectory *Laser Photon. Rev.* **2024** 2301372
[32] Fu B Y, Li T, Zou X, Ren J, Yuan Q, Wang S, Cao X and Wang Z 2022 Steerable chromatic dispersive metalenses in dual bands *J. Appl. Phys.* **55** 255105
[33] Chen R, Bi Q, Li T, Wang S, Zhu S and Wang Z 2023 Dual-wavelength chiral metasurfaces based on quasi-bound states in the continuum *J. Opt.* **25** 045001
[34] Neshev D N and Miroshnichenko A E 2023 Enabling smart vision with metasurfaces *Nat. Photon.* **17** 26–35
[35] Rao S J, Huang Y, Cui K and Li Y 2022 Anti-spoofing face recognition using a metasurface-based snapshot hyperspectral image sensor *Optica* **9** 1253–9
[36] Wu Z P, Zhang Z, Xu Y, Zhai Y, Zhang C, Wang B and Wang Q 2022 Random color filters based on an all-dielectric metasurface for compact hyperspectral imaging *Opt. Lett.* **47** 4548–51
[37] Duarte M F and Eldar Y C 2011 Structured compressed sensing: from theory to applications *IEEE Trans. Signal Process.* **59** 4053–85
[38] Barnes W L, Dereux A and Ebbesen T W 2003 Surface plasmon subwavelength optics *Nature* **424** 824–30
[39] Nie S M and Emory S R 1997 Probing single molecules and single nanoparticles by surface-enhanced Raman scattering *Science* **275** 1102–6
[40] Zhu J and Li N 2020 MIM waveguide structure consisting of a semicircular resonant cavity coupled with a key-shaped resonant cavity *Opt. Express* **28** 19978–87
[41] Tian M, Lu P, Chen L, Liu D and Peyghambarian N 2012 Plasmonic Bragg reflectors based on metal-embedded MIM structure *Opt. Commun.* **285** 5122–7